IEEE Access
Multidisciplinary : Rapid Review : Open Access Journal

Received February 28, 2020, accepted March 12, 2020, date of publication March 16, 2020, date of current version March 26, 2020.

Digital Object Identifier 10.1109/ACCESS.2020.2981041

Design of Combined Printed Helical Spiral Antenna and Helical Inverted-F Antenna for Unmanned Aerial Vehicle Application

YUNAN HAN[1], (Member, IEEE), KUNKUN HU[1], RUICHUN ZHAO[2], YUAN GAO[1], LIN DAI[3], YUFENG FU[1], BOWEN ZHOU[1], AND SIYU YUAN[4]

[1]College of Information Science and Technology, Beijing University of Chemical Technology, Beijing 100029, China
[2]College of Materials Science and Engineering, Beijing University of Chemical Technology, Beijing 100029, China
[3]Liaohe Petroleum Exploration Bureau Communication Company, Panjin 124010, China
[4]Beijing Key Laboratory of Intelligent Telecommunications Software and Multimedia, Beijing University of Posts and Telecommunications, Beijing 100876, China

Corresponding author: Yunan Han (clark-han@139.com)

This work was supported in part by the Beijing Natural Science Foundation under Grant 8202036, in part by the National Natural Science Foundation of China under Grant 21656001, and in part by the Open Foundation of State Key Laboratory of Networking and Switching Technology, Beijing University of Posts and Telecommunications, under Grant SKLNST-2018-1-02.

ABSTRACT The design and implementation of printed helical spiral antenna (PHSA) and helical printed inverted-F antenna (IFA) are presented for unmanned aerial vehicle (UAV) with global positioning system (GPS) $L1$ band (1.57 GHz) and telemetry communication frequency band (2.33 GHz) applications. The proposed antenna is miniaturized by co-winding the radiation elements on the same ceramic rod, surface covering by dielectric sealant, inserting a high permittivity dielectric load into the helical structure, turning and meandering the radiation element of PHSA into a spiral parallelogram structure. The PHSA and helical IFA antenna radiation elements are manufactured by silver pasted on the same hollow ceramic cylinder with a diameter of 12 mm and a height of 24.7 mm. The experimental and simulation results show that the proposed PHSA and IFA can achieve the gain of 0.05dB and 1.97 dB respectively and be suitable for GPS $L1$ band and telemetry communication frequency band (2.33 GHz) applications separately.

INDEX TERMS Circular polarization, GPS antenna, helical inverted-F antenna, printed spiral helical antenna, unmanned aerial vehicle.

I. INTRODUCTION

With the development of Unmanned Aerial Vehicle (UAV) technology, the requirement of airborne communication equipment is further improved. The antennas of UAVs are usually extremely important components for global positioning navigation and telemetry communication applications. During the operation of UAVs, the position information of the UAV can be obtained by GPS positioning, and the control signal can be obtained by telemetry communication. The two functions of UAV communication equipment are provided by two antennas respectively, but miniaturized UAVs are usually affected by aerodynamics, structural mechanics, electromagnetic compatibility and other factors, which cannot provide separate installation space for the two antennas. Moreover, due to the influence of the structure of such aircraft, the antenna position and volume requirements are also relatively high. Therefore, the combination of two antennas in one antenna module is a very possible candidate solution to this requirement.

GPS antenna is a key component for UAVs to receive signals from GPS orbiting satellites. Due to the insensitivity to the rotation of ionospheric polarization, the GPS antenna is required to have right circular polarization (CP) and a uniform mode covering the entire upper hemisphere. In previous studies on GPS antennas, quadrifilar helical antennas (QHA) are well studied [1]–[5], which usually have good CP performance. Improved from QHA, a printed quadrifilar helical antenna (PQHA) was developed with four radiation elements printed on flexible dielectric substrate [6]–[9]. To meet the requirement of antenna miniaturization, a folded printed quadrifilar helical antenna (FPQHA) is developed with the

The associate editor coordinating the review of this manuscript and approving it for publication was Yingsong Li.

advantages of good CP performance, light weight and good axial ratio [10]–[15].

Telemetry communication antenna is the key component of transmitting and receiving ground control signal for UAV. Telemetry communication band is usually allocated in S band. In many previous researches, some telemetry antennas with excellent performance are proposed, such as telemetry loaded bifilar helical antenna [16], flush-mounted telemetry antenna [17], compact S-band antenna [18] and hybrid TM antenna [19]. Inverted-F antenna (IFA) [20]–[24] is also a very possible candidate for this application. In general, the radiation elements of IFA and the ground plane are fabricated on traditional printed circuit board (PCB) with planar structure [25] [26]. To meet the design requirements, the planar IFA radiation elements can be made perpendicular to the ground [27]. These planar IFA design methods described above indicated that three main structural parameters which can determine the antenna's input impedance, resonance frequency, impedance bandwidth and other performance. The three main structural parameters of the planar IFA are the resonant length L, the height H and the space distance S between the two vertical arms. By adjusting the three structural parameters, planar IFA can be easily designed and optimized.

Although the structure of FPQHA and planar IFA is already very small, the applications on UAV still puts forward higher requirements on miniaturization of antenna system. Recently, several methods of antenna miniaturization are developed, including inserting dielectric loading [28], folding the helix antenna arms [29] [30], applying different helix turn angles [31], using stepped-width arms [32], using impedance matching network[33] and power divider networks [34].

In this paper, a design of combined printed helical spiral antenna and helical inverted-F antenna is presented for unmanned aerial vehicle application. Improving the dual-arm spiral GPS antenna [35], the original GPS antenna is retained by one radiation element left and the telemetry communication function is added. PHSA fits GPS L1 (1.575 GHz) band, and helical IFA fits telemetry communication frequency band (S band) separately. The structural parameters are optimized to obtain dual frequency band and right-hand CP performance, and the influence of IFA arm length, space between the two radiation elements and loading ceramic cylinder thickness on resonant frequency of the proposed antenna was simulated and compared. Meanwhile, an optimized design is fabricated and measured, and the experimental results are well compared with simulation to verify the design. The proposed antenna can be used in UAV to build wireless senor network in oil field. Due to the high flying of UAV, it can collect the information of wireless sensor network nodes in a long distance.

II. ANTENNA DESIGN

A. ANTENNA CONFIGURATION

The proposed PHSA and helical IFA mounting on a type of UAV is shown in Fig. 1(a), where the proposed PHSA and helical IFA radiation elements are printed on the Al_2O_3 ceramic rod as shown in Fig. 2(b). In order to guarantee the strength of the overall structure, the ceramic rod is screwed on the aluminum base of canards by metal bolt and the proposed antenna surface covered with sealant, therefore it can handle the acceleration overload during flight. At the same time, the radome's structure is streamlined in order to reduce air resistance, and sealant can guarantee the high-grade sealing and heat conduction. The coaxial cables of 50 ohm are used for feeding, one end of the inner conductor is welded on the end of feeding line of the proposed PHSA and the helical IFA separately, and the outer conductors are welded on the small rectangular plate extending from ground. The other end of the feed coaxial cables with IPEX III connectors are connected to the circuit PCB down the base of canards through the through-holes on the lower part of the aluminum base.

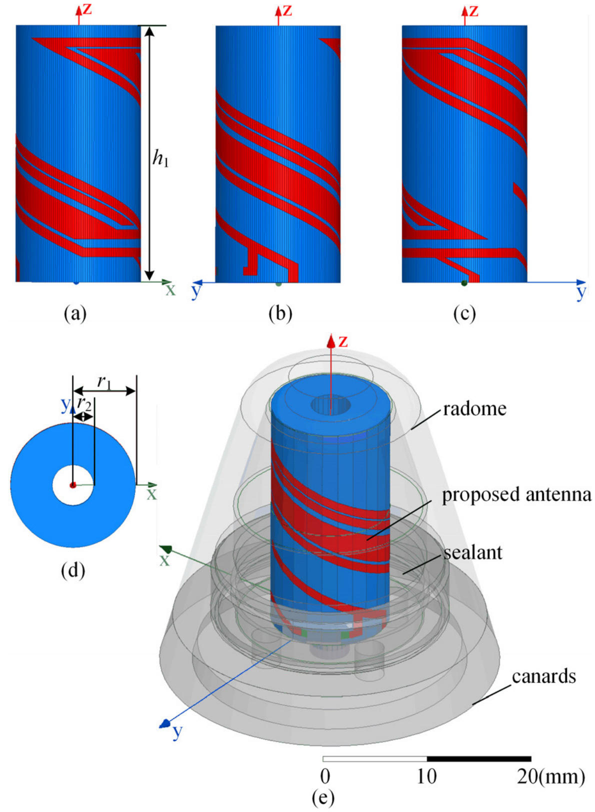

FIGURE 1. Geometry of the proposed PHSA and helical IFA. (a) Front view, (b) left view, (c) right view, and (d) vertical view of the proposed PHSA and helical IFA radiation elements printed on the Al_2O_3 ceramic rod. (e) The proposed PHSA and helical IFA mounting on UAV.

The proposed PHSA and helical IFA radiation elements are printed on the Al_2O_3 ceramic rod with a radius of $r_1 = 6$ mm, a coaxial M4 screw hole of $r_2 = 2$ mm and a height of $h_1 = 24.7$mm. The ceramic rod working as substrate is made of material with high relative permittivity and low dissipation factor. According to previous studies, substrate made of high relative permittivity material can effectively reduce the resonant frequency of the antenna. The ceramic rod in this study is with relative permittivity of $\varepsilon_r = 9.8$ and dissipation factor of loss tan $\delta = 0.0001$ at 10 GHz. The relative permittivity of

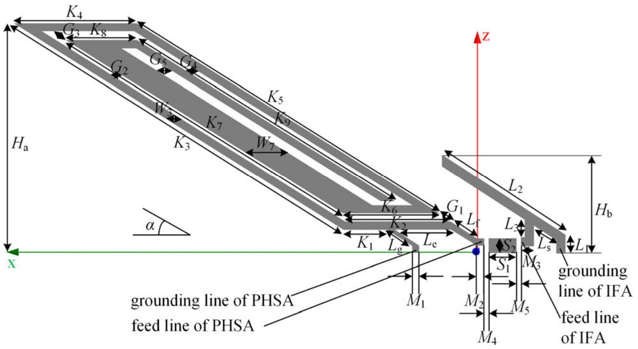

FIGURE 2. Layout of the proposed unwrapped PHSA and helical IFA.

the sealant covered the proposed antenna is $\varepsilon_r = 4.1$, and the material of the radome is BN with relative permittivity $\varepsilon_r = 4$. The bottom of the ceramic rod is printed with silver, and the contact surface of the aluminum base has good electrical conductivity without surface oxidation, which can be used as the ground for the antenna.

Fig. 2 shows the layout of the proposed unwrapped PHSA and helical IFA. The radiation element on the left is PHSA, which is applied to the GPS frequency band. The radiation element on the right is the helical IFA, which is used for the telemetry communication frequency band (2.33 GHz). The unwrapped PHSA radiation elements consists of a feeding line, a grounding line, and a radiation line with turning and meandering helix arm into the form of an end-to-end 8 silver microstrips parallelogram spiral with length form K_2 to K_9.

In order to optimize the manufacturing process, the traditional PQHA feed direction is improved, and the vertical feed is changed to the parallel feed, and a rectangular grounding plate with length S_1 and width S_2 is added. The feeding line with length L_f is connected at the end of the radiation element, and has a gap M_4 with a rectangular grounding plate which is connected to the ground at the bottom of the rod. The grounding line with length L_g is connected with the first radiation part and the ground at the bottom of the rod, and it is used to improve the characteristic impedance of the proposed PHSA. The IPEX III coaxial cable with 50 Ohm impedance is used for feeding, then the inner conductor is welded on the extended part of feeding line with length L_f, and the outer conductor is welded on the rectangular grounding plate. The rectangular grounding plate is very close to the proposed PHSA and the proposed helical IFA with gaps of M_2 and M_3 separately. The main radiation part with length L_2 of the proposed helical IFA has the same pitch angle α as the proposed PHSA. The ground line of the proposed helical IFA with length L_1 is vertically connected the main radiation part with the ground at the bottom of the rod. The feed line with length L_3 is paralleled to the ground line with distance of L_s. The inner conductor of IPEX III coaxial cable is welded on the extended part of feeding line with length L_3, and the outer conductor is welded on the rectangular grounding plate. The feeding lines for the proposed PHSA and the proposed helical

TABLE 1. Geometrical parameters of proposed PHSA and helical IFA.

Parameters	Value (mm)	Parameters	Value (mm)
h_1	24.7	G_4	0.5
H_a	23.5	G_5	1.5
H_b	9.7	K_1	6.1
M_1	1	K_2	14.6
M_2	1	K_3	48.1
M_3	1.5	K_4	15
M_4	0.7	K_5	44.1
M_5	0.7	K_6	12.2
L_1	1.8	K_7	41.7
L_2	17.3	K_8	9.7
L_3	1.8	K_9	38.7
L_e	7.9	r_1	6
L_f	4.1	r_2	2
L_g	3.8	S_1	3.5
L_s	3.4	S_2	1.5
G_1	2	W_3	2
G_2	0.8	W_7	6.2
G_3	0.4		

α=26º
L_a =arm length of the proposed PHSA.
$L_a = M_2 + L_f + K_2 + K_3 + K_4 + K_5 + K_6 + K_7 + K_8 + K_9 - 6W_3 - 2W_7 = 204.8$ mm.

IFA can pass through the hole of the aluminum base and connect with the RF circuits.

B. ANTENNA PARAMETERS

The geometrical parameters of the proposed PHSA and helical IFA can be optimized by electromagnetic simulation tool high frequency structure simulation software (HFSS) [36] as shown in Table 1.

C. THEORY ANALYSIS

The following relations [11] can calculate the arm length (L_a) of the proposed PHSA:

$$L_a = \frac{c\,(2n+1)}{4f\sqrt{\varepsilon_{\text{reff}}}} \tag{1}$$

where c is light speed in free space, n is nature number corresponding to the number of harmonics resonate frequency, f is the operating frequency and $\varepsilon_{\text{reff}}$ is the equivalent effective relative dielectric permittivity of the dielectric substrate.

For the proposed helical IFA, the initial antenna structure parameters can be obtained from the empirical formula [21]:

$$L_2 - L_s + L_1 \approx \frac{c}{4f\sqrt{(1+\varepsilon_{\text{reff}})/2}} \tag{2}$$

where $L_2 - L_s + L_1$ is the resonant length of antenna.

D. ANTENNA DESIGN PROCEDURE

The arm length (L_a) of proposed PHSA can be calculated by Equ. 1, where f is the operating frequency at GPS $L1$ band (1.575 GHz), $\varepsilon_{\text{reff}}$ is the equivalent effective relative dielectric permittivity of the dielectric substrate.

TABLE 2. The arm length (L_a) for GPS $L1$ band.

N	L_a (mm)	n	L_a (mm)
1	48.1	5	176.4
2	80.2	6	**208.4**
3	112.2	7	240.5
4	144.3	8	272.6

The equivalent effective relative permittivity ε_{reff} of the ceramic rod is determined from [36]

$$\varepsilon_{reff} = \left[1 - \left(\frac{r_2}{r_1}\right)^2\right]\varepsilon_r + \left(\frac{r_2}{r_1}\right)^2 \quad (3)$$

where relative permittivity $\varepsilon_r = 9.8$ for Al_2O_3 ceramic rod, radius $r_1 = 6$ mm, coaxial M4 screw hole $r_2 = 2$ mm. Then the equivalent effective relative permittivity ε_{reff} is 8.82.

Calculated by Equ. 1, Table 2 shows the possible arm length (L_a) of the proposed PHSA. The arm length L_a = 208.4 mm is considered to turn into parallelogram spiral with end-to-end 9 silver strips. The radiation part of PHSA need to turn the arm into the form of a parallelogram spiral and wrap around the cylinder, therefore, the arm length is the total length of the end-to-end 9 silver strips, minus the length of the 8 corners generated by the bending process, i.e

$$L_a = M_2 + L_f + K_2 + K_3 + K_4 + K_5 + K_6 + K_7 + K_8 + K_9 - 6W_3 - 2W_7 \quad (4)$$

The arm length in Fig. 1 and Table 1 simulated by HFSS is 204.8 mm which is a little bit shorter than calculated 208.4 mm, because the antenna is covered by sealant and radome.

The arm length (L_2–L_s + L_1) of proposed IFA can be calculated by Equ. 2, where f is the operating frequency at telemetry communication frequency band (2.33 GHz), ε_{reff} is the equivalent effective relative dielectric permittivity of the dielectric substrate calculated by equ. 3. The calculated arm length $L_2 - L_s + L_1 \approx 14.5$ mm is considered in simulation. Simulated by HFSS, we can obtain $L_2 = 17.3$ mm, $L_s = 3.4$ mm, and $L_1 = 1.8$ mm for this application, $L_2 - L_s + L_1 = 15.7$ mm which is a little bit longer than 14.5, because the proposed IFA is spirally wound on the ceramic rod compared with traditional planar IFA.

The proposed PHSA and helical IFA are designed and simulated by HFSS, and the optimized parameters can be achieved as shown in Fig.7 according to the antenna parameters in Table 1. Deduced from Euq. 1, all the resonance frequency of the proposed FHSA with arm length (L_a) is

$$f_n = \frac{c}{\sqrt{\varepsilon_{reff}}}\frac{(2n+1)}{4L_a} \quad (5)$$

Similarly, all the resonance frequency of the proposed helical IFA can be deduced from Euq. 2.

$$f_n \approx \frac{nc}{(L_2 - L_s + L_1)\sqrt{(1+\varepsilon_{reff})/2}} \quad (6)$$

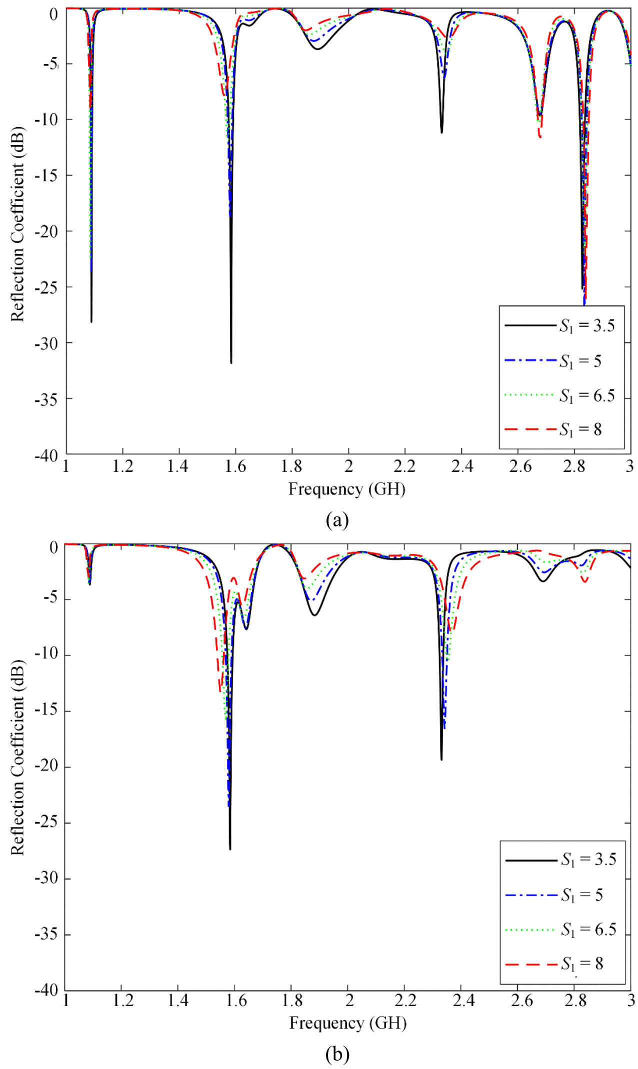

FIGURE 3. Simulated reflection coefficient versus frequency for the space between the two radiation elements (various values of S_1). (a) The proposed PHSA. (b) The proposed helical IFA.

The proposed PHSA has multiple resonant frequency bands, for GPS L1 band $f_1 = 1.575$ GHz, the reflection coefficient $S_{11} = -23.7$ dB as shown in Fig. 7(a). The proposed helical IFA has two resosnant frequency bands within the range of 1-3GHz, in which the resonant frequency $f_2 = 2.33$ GHz and the reflection coefficient $S_{22} = -35.9$ dB, which can meet the requirements of the telemetry frequency band as shown in Fig. 7(b).

III. PARAMETER STUDY

In this study, the proposed PHSA and helical IFA is optimized by considering the effect of the spacing "S_1" between the two radiation elements, the arm length "L_2" of the proposed IFA and the inner hole radius "r_2" of the ceramic rod while the other parameters remain unchanged as in Table 1.

A. EFFECT OF THE SPACE BETWEEN THE TWO RADIATION ELEMENTS

The variation of "S_1", the space between the two radiation elements, is considered to study the effect on the proposed

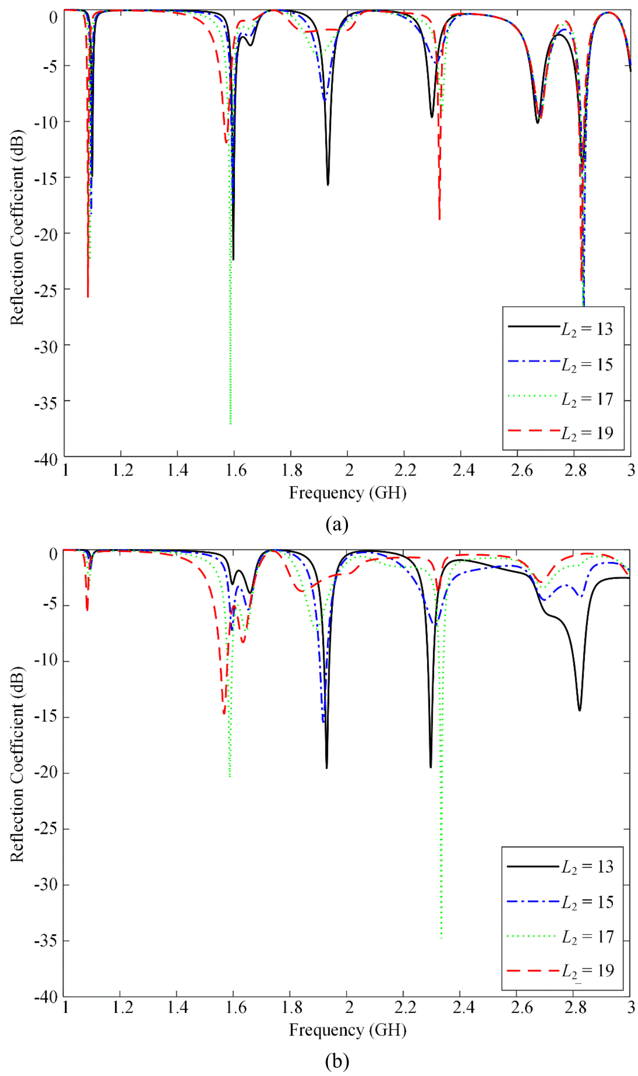

FIGURE 4. Simulated reflection coefficient versus frequency for the arm length of the proposed IFA (various values of L_2). (a) The proposed PHSA. (b) The proposed helical IFA.

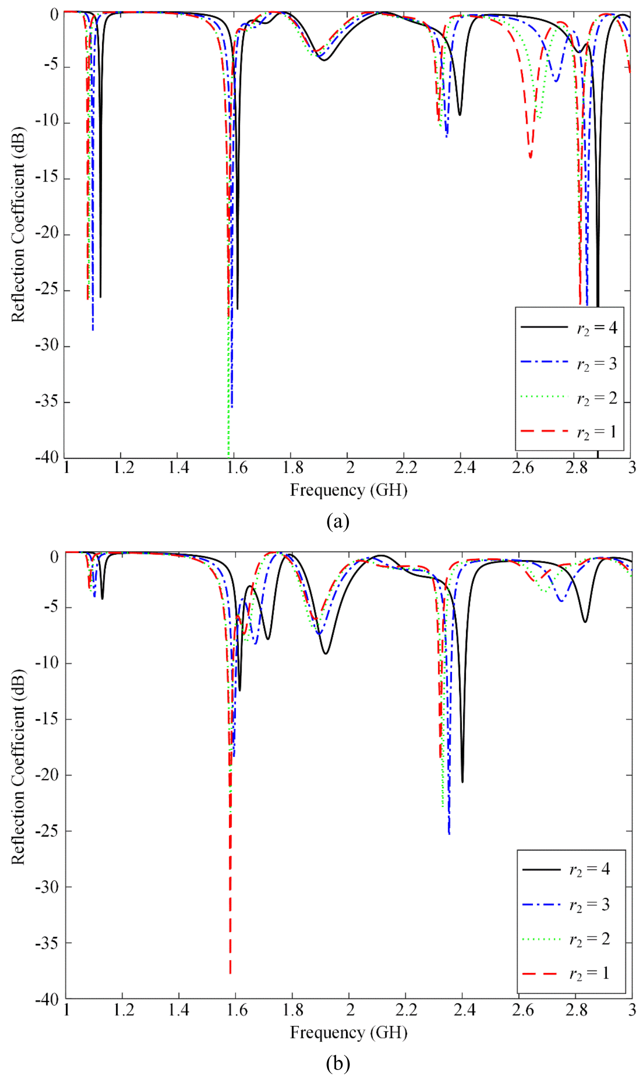

FIGURE 5. Simulated reflection coefficient versus frequency for the thickness of the ceramic cylinder (various values of r_2). (a) The proposed PHSA. (b) The proposed helical IFA.

PHSA and helical IFA. In Fig. 3, the reflection coefficients versus frequency are presented for different values of S_1(S_1 = 3.5, 5, 6.5, and 8 mm). With the increase of S_1, the resonant frequency slightly decreases for both the proposed PHSA and helical IFA within the frequency range of 1 GHz to 3 GHz as shown in Fig. 3(a) and Fig. 3(b).

B. EFFECT OF THE PROPOSED IFA ARM LENGTH

Considering the variation of "L_2", the arm length of the proposed helical IFA, the influence on the resonate frequency is studied for the proposed helical IFA and the proposed PHSA. In Fig. 4, the reflection coefficients versus frequency are presented for different values of L_2 (L_2 = 13, 15, 17, and 19 mm) respectively, while the other structural parameters are fixed as table 1. The change of L_2 has little effect on the resonant frequency in the 1-3 GHz range of the proposed PHSA, but has significant effects on the resonance frequency of the proposed helical IFA. Therefore, in the case of antenna parameter optimization, the proposed helical IFA performance can be adjusted without affecting the proposed PHSA.

C. EFFECT OF THE CERAMIC ROD INNER HOLE

The variation of "r_2" (r_2 = 4, 3, 2, and 1 mm) is simulated to consider the effect of the inner hole radius of the ceramic rod. The reflection coefficient versus frequency associated with different r_2 is shown in Fig. 5. As the value of r_2 decreases, the thickness of the substrate increases and the resonant frequency of the proposed PHSA and helical IFA decreases. Therefore, it is very important to select appropriate ceramic coaxial hole radius "r_2", so that both the proposed PHSA and helical IFA can achieve an ideal reflection coefficient in the corresponding resonance frequency. When r_2 = 2 mm, the reflection coefficient of the PHSA at GPS L1 (1.575 GHz) band reaches the maximum bandwidth. When r_2 = 3 mm, the reflection coefficient of the helical IFA at 2.33GHz reaches

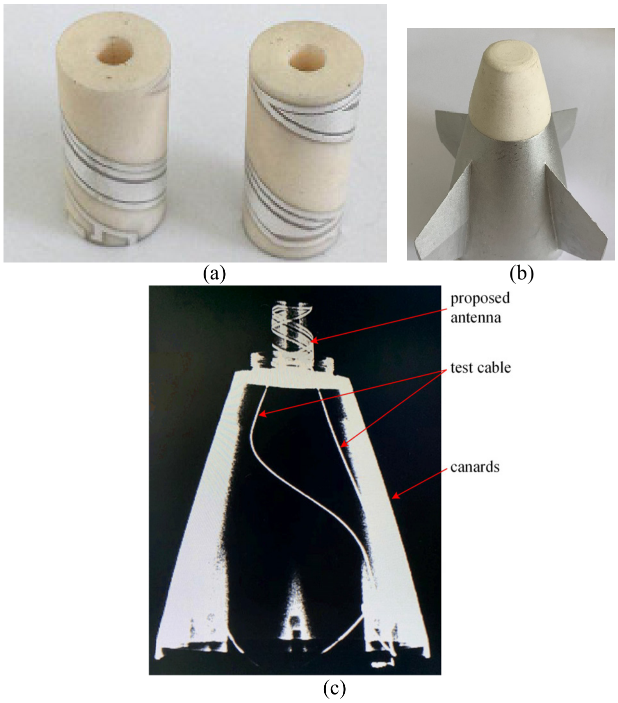

FIGURE 6. **Photo of the proposed PHSA and helical IFA. (a) The proposed PHSA and helical IFA printed on ceramic rod. (b) The proposed PHSA and helical IFA mounting on UAV covered by sealant and coated by radome. (C) X-ray photographs of the proposed PHSA and helical IFA mounting on UAV.**

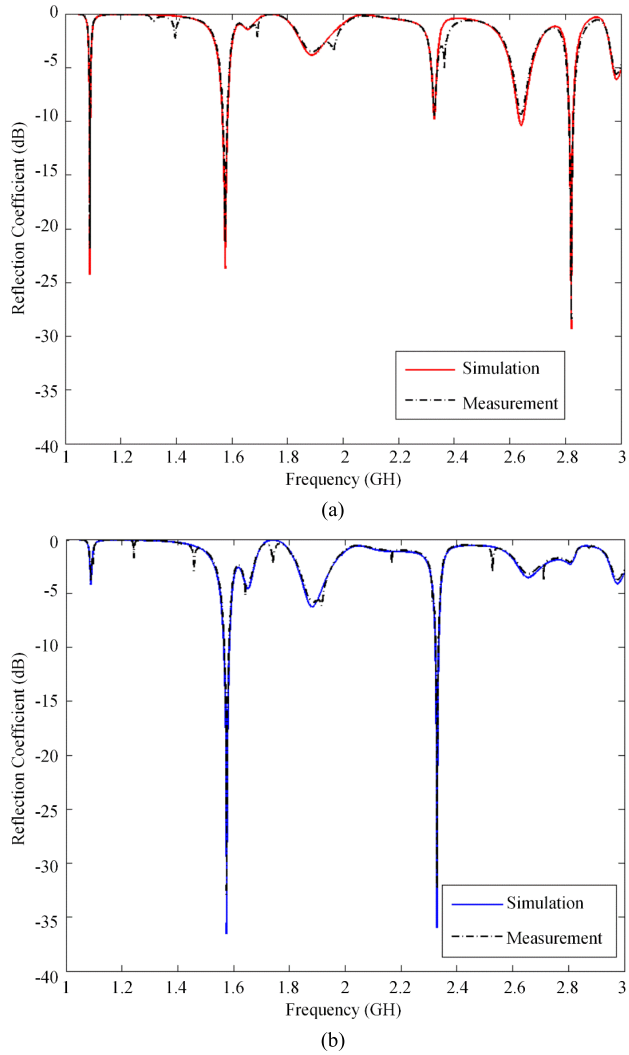

FIGURE 7. **Comparison of measured and simulated reflection coefficient versus frequency of the proposed PHSA and helical IFA. (a) Reflection coefficient of the proposed PHSA. (b) Reflection coefficient of the proposed helical IFA.**

the maximum bandwidth. Considering the performance of the two radiation elements, $r_2 = 2$ mm is selected to achieve better performance of the antenna system.

IV. EXPERIMENTAL RESULTS

The proposed PHSA and helical IFA has been not only manufactured by printing silver on ceramic rod, but also mounted on a typical UAV covered by sealant and coated by radome, as shown in Fig. 6(a) and Fig. 6(b) separately.

The reflection coefficient versus frequency of the proposed PHSA and helical IFA mounting on UAV covered by sealant and coated by radome is measured by the Keysight N5245A (Calibrated by N4691-40004) PNA network analyzer separately. The measured and simulated reflection coefficient versus frequency of the proposed PHSA and helical IFA mounting on unmanned platform is shown in Fig. 7. We can notice that the reflection coefficient versus frequency curves measured by the network analyzer and simulated by HFSS agree well with each other. The bandwidth is about 20 MHz (1.565-1.585 GHz) for GPS $L1$ band and 14 MHz (2.322-2.336 GHz) for telemetry communication frequency band.

There are different requirements for antenna radiation pattern when mounting on different type of UAV. In this case, the GPS antenna and telemetry communication antenna must be merged into one unit and the antenna structure must be compact enough to put inside the radome. Moreover, the metal structure of UAV is very close to the antenna, the antenna design and antenna distribution on UAV must be carried out through the cooperative simulation of UAV and GPS antenna together.

The radiation pattern measurement setup of the proposed PHSA and helical IFA mounting on UAV at anechoic chamber is shown in Fig. 8. As shown in Fig. 9 and Fig. 10, the measured gain values anastomose well with simulation in radiation pattern. It can be concluded from the radiation pattern that in GPS $L1$ (1.575 GHz) band, the PHSA has nearly spherical shape radiation patterns with circular polarization in the xoy-plane, xoz-plane and yoz-plane. The nearly omnidirectional radiation pattern can be noticed with good cross-polar performance. The maximum radiation direction is about $\theta = 90°$, $\varphi = 310°$, and the gain is about 0.05 dB. In Fig. 9, the measured radiation patterns compared to the simulated ones are shown for telemetry communication frequency band. Fig. 9 (b) and (c) shown the helical IFA has quite omnidirectional radiation patterns in the

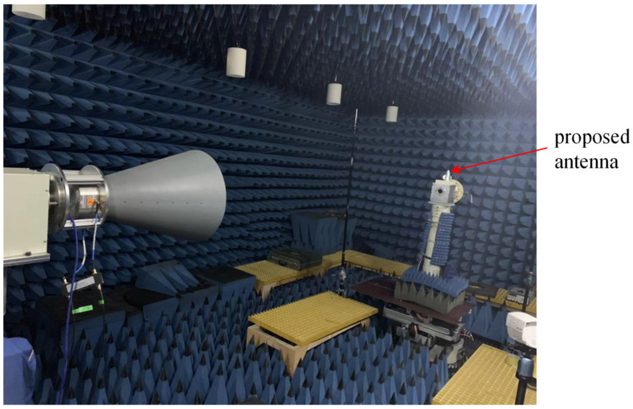

FIGURE 8. Measurement setup of radiation pattern at anechoic chamber.

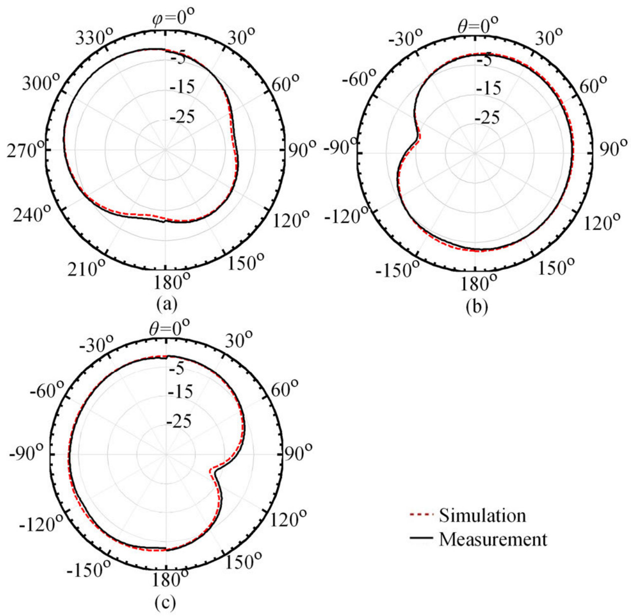

FIGURE 9. Comparison of measured and simulated radiation patterns of the proposed PHSA and helical IFA at GPS L1 (1.575 GHz) band. (a) xoy-plane; (b) xoz-plane; (c) yoz-plane.

xoz-plane and yoz-plane. The maximum radiation direction is $\theta = 60°$ and $\varphi = 270°$, and the gain is about 1.97 dB. It can be considered that the proposed PHSA and helical IFA can receive GPS and telemetry communication signals very well, though UAV platform is in any position of the moving trail.

The measured axial ratio (AR) of the proposed PHSA and helical IFA at GPS L1 (1.575 GHz) band and telemetry communication frequency band (2.33 GHz) respectively is shown in Fig. 11 at xoz-plane (Phi = 0°), at yoz-plane (Phi = 90°) and at xoy-plane (Theta = 90°). We can notice that most of the axial ratio is less than 3 dB.

Some referenced PQHAs are shown in Table 3, and the performance comparison is considered with the proposed PHSA and helical IFA. Based on co-winding the radiation elements on the same ceramic rod, covering the radiation

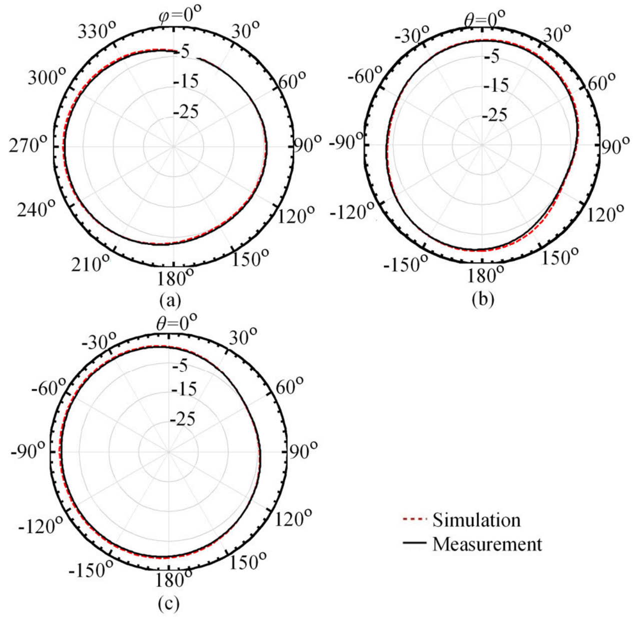

FIGURE 10. Comparison of measured and simulated radiation patterns of the proposed PHSA and helical IFA at telemetry communication frequency band (2.33 GHz). (a) xoy-plane; (b) xoz-plane; (c) yoz-plane.

TABLE 3. Performance comparisons among the reported antenna.

Ref.	Operating frequency (GHz)	Size (mm)	Structure	Gain (dB)	AR (dB)	substrate
this work	1.565-1.585/ 2.322-2.336	ϕ12×24.7H	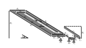	0.05/ 1.97	3	Al_2O_3 ceramic ($\varepsilon_r = 9.8$)
[7]	1.25-1.29/1.43-1.47 /1.68-1.72	ϕ36×115H	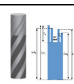	1.5	3	Neltec ($\varepsilon_r = 2.2$)
[9]	1.2-1.28/ 1.4-1.5	ϕ30×113H		2/4	3	Neletc ($\varepsilon_r = 2.2$)
[12]	1.2-1.24/1.56-1.59/1.82-1.84	ϕ36×78H	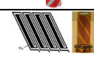	4.6/ 1.4/ 2.5	3	Nelect ($\varepsilon_r = 2.2$)
[13]	1.25-1.27/ 1.56-1.58	ϕ36×57H		3.76/ 1.06	3	Neltec ($\varepsilon_r = 2.2$)
[14]	1.22-1.24/ 1.56-1.58	ϕ30×85H	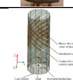	4.44/ 3.87	3.2/6	Rogers RT/duroid 5880 (tm) ($\varepsilon_r = 2.2$)
[18]	1.98-2.35	ϕ86×12H	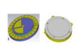	9	2-6	Foam material (ε_r = 1.06)
[32]	1.1-1.3/ 1.5-1.6	ϕ44.7×81.6 H	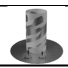	6.3/ 6.4	3	PET ($\varepsilon_r = 2.3$)

elements by dielectric sealant, inserting dielectric loading inside the helix, the proposed antenna for UAV application has smaller size (ϕ12 mm × 24.7 mm), dual frequency band, low weight (11 g) and very good structural strength. Most of PQHAs are fabricated by flexible dielectric substrate such as polyimide film, foam, Rogers RT/duroid or liquid crystal polymer (LCP) film, etc. The flexible substrate with lower

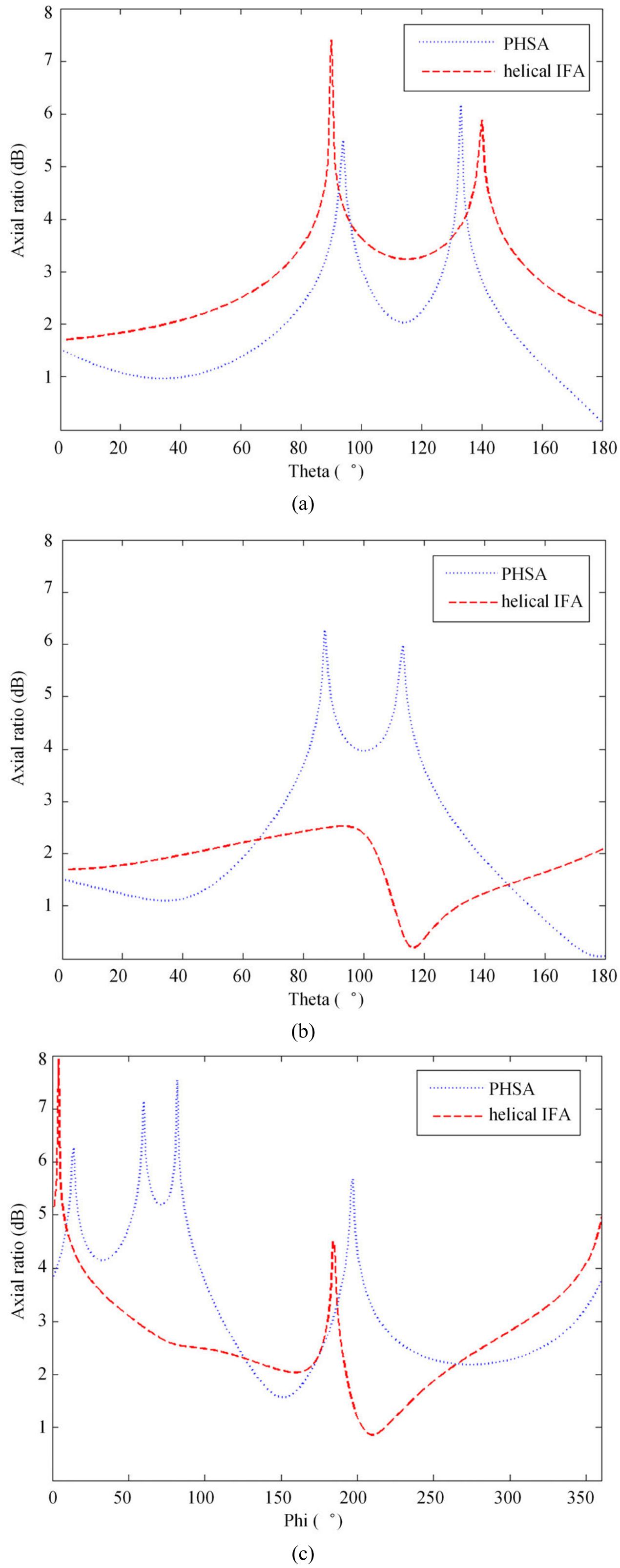

FIGURE 11. **Measured axial ratio of the proposed PHSA and helical IFA at GPS L1 (1.575 GHz) band and telemetry communication frequency band (2.33 GHz) respectively. (a) at xoz-plane (Phi = 0°); (b) at yoz-plane (Phi = 90°); (c) at xoy-plane (Theta = 90°).**

relative permittivity, which limited the antenna application by larger size and lower structure strength.

V. CONCLUSION

In this paper, a printed helical spiral antenna and helical inverted-F antenna working in GPS $L1$ band(1.57 GHz) and telemetry communication S band (2.33 GHz) are designed and fabricated for the application of UAV. The structure of the proposed PHSA and helical IFA is miniaturized by co-winding the radiation elements on the same ceramic rod, surface covering by dielectric sealant, turning and meandering the radiation elements into spirals. The proposed PHSA and helical IFA is fabricated by printing silver strips on a ceramic hollow rod substrate with a height of 24.7 mm and a diameter of 12 mm. The proposed antenna can achieve the bandwidth of is about 20 MHz and 14 MHz (2.322-2.336 GHz) (1.565-1.585 GHz) the gain of 0.05dB and 1.97 dB for GPS L1 band and for telemetry communication frequency band respectively. The measured and simulated results of reflection coefficient and radiation patterns fit very well, which validates the design methods and suggests that PHSA and helical IFA is suitable for UAV applications.

REFERENCES

[1] J. Costantine, Y. Tawk, I. Maqueda, M. Sakovsky, G. Olson, S. Pellegrino, and C. G. Christodoulou, "UHF deployable helical antennas for CubeSats," *IEEE Trans. Antennas Propag.*, vol. 64, no. 9, pp. 3752–3759, Sep. 2016.

[2] X. Bai, J. Tang, X. Liang, J. Geng, and R. Jin, "Compact design of triple-band circularly polarized quadrifilar helix antennas," *IEEE Antennas Wireless Propag. Lett.*, vol. 13, pp. 380–383, 2014.

[3] J. M. Tranquilla and S. R. Best, "A study of the quadrifilar helix antenna for global positioning system (GPS) applications," *IEEE Trans. Antennas Propag.*, vol. 38, no. 10, pp. 1545–1550, Oct. 1990.

[4] S. R. Best, "A 7-turn multi-step quadrifilar helix antenna providing high phase center stability and low angle multipath rejection for GPS applications," in *Proc. IEEE Antennas Propag. Soc. Symp. (APS/URSI)*, Monterey, CA, USA, Jun.2004, pp. 2899–2902.

[5] D. Lamensdorf and M. A. Smolinski, "Dual-band quadrifilar helix antenna," in *Proc. IEEE Int. Symp. Antennas Propag.*, San Antonio, TX, USA, Jun. 2002, pp. 488–491.

[6] Y. Tawk, M. Chahoud, M. Fadous, J. Costantine, and C. G. Christodoulou, "Miniaturization of a partially 3-D printed quadrifilar helix antenna," *IEEE Trans. Antennas Propag.*, vol. 65, no. 10, pp. 5043–5051, Oct. 2017.

[7] Y. Letestu and A. Sharaiha, "Multiband printed quadrifilar helical antenna," *Electron. Lett.*, vol. 46, no. 13, pp. 885–886, 2010.

[8] Y.-S. Wang and S.-J. Chung, "A miniature quadrifilar helix antenna for global positioning satellite reception," *IEEE Trans. Antennas Propag.*, vol. 57, no. 12, pp. 3746–3751, Dec. 2009.

[9] A. Sharaiha and Y. Letestu, "Quadrifilar helical antennas: Wideband and multiband behavior for GPS applications," in *Proc. Int. Conf. Electromagn. Adv. Appl.*, Sydney, NSW, Australia, Sep. 2010, pp. 620–623.

[10] J. M. O'Brien, J. E. Grandfield, G. Mumcu, and T. M. Weller, "Miniaturization of a spiral antenna using periodic Z-plane meandering," *IEEE Trans. Antennas Propag.*, vol. 63, no. 4, pp. 1843–1848, Apr. 2015.

[11] J. Rabemanantsoa and A. Sharaiha, "Size reduced multi-band printed quadrifilar helical antenna," *IEEE Trans. Antennas Propag.*, vol. 59, no. 9, pp. 3138–3143, Sep. 2011.

[12] Y. Tawk, M. Chahoud, M. Fadous, J. Costantine, and C. G. Christodoulou, "Miniaturization of a partially 3-D printed quadrifilar helix antenna," *IEEE Trans. Antennas Propag.*, vol. 65, no. 10, pp. 5043–5050, Oct. 2017.

[13] J. Rabemanantsoa and A. Sharaiha, "Dual-band meandered folded printed quadrifilar helix antenna," in *Proc. 4th IEEE Int. Symp. Microw., Antenna, Propag. EMC Technol. Wireless Commun.*, Beijing, China, Nov. 2011, pp. 91–94.

[14] Y.-H. Yang, J.-L. Guo, B.-H. Sun, and Y.-H. Huang, "Dual-band slot helix antenna for global positioning satellite applications," *IEEE Trans. Antennas Propag.*, vol. 64, no. 12, pp. 5146–5152, Dec. 2016.

[15] S. Khajepour, M. S. Ghaffarian, and G. Moradi, "Design of novel multi-band folded printed quadrifilar helical antenna for GPS/WLAN applications," *Electron. Lett.*, vol. 53, no. 2, pp. 58–60, Jan. 2017.

[16] D. Colantonio and C. Rosito, "A spaceborne telemetry loaded bifilar helical antenna for LEO satellites," in *Proc. SBMO/IEEE MTT-S Int. Microw. Optoelectron. Conf. (IMOC)*, Belem, Brazil, Nov. 2009, pp. 741–745.

[17] P. C. R. Filho, A. F. Tinoco-S., D. C. Nascimento, and J. C. da S. Lacava, "Flush-mounted telemetry antenna design for a sounding rocket competition," in *Proc. IEEE Antennas Propag. Soc. Int. Symp. (APSURSI)*, Orlando, FL, USA, Jul. 2013, pp. 2173–2174.

[18] A. Bellion, K. Elis, and S. De Gaetano, "New compact S-band antenna for nanosatellite TeleMetry and TeleCommand applications–EyeSat program," in *Proc. 10th Eur. Conf. Antennas Propag. (EuCAP)*, Davos, Switzerland, Apr. 2016, pp. 1–5.

[19] N. Lecerf, S. Villers, and J. Dugenet, "New concept of small antennas for telemetry and tracking trajectory on space reentry vehicles," in *Proc. 8th Eur. Conf. Antennas Propag. (EuCAP)*, The Hague, The Netherlands Apr. 2014, pp. 2067–2070.

[20] C. Soras, M. Karaboikis, G. Tsachtsiris, and V. Makios, "Analysis and design of an inverted-F antenna printed on a PCMCIA card for the 2.4 GHz ISM band," *IEEE Antennas Propag. Mag.*, vol. 44, no. 1, pp. 37–44, Feb. 2002.

[21] B. Gowrish, D. John, D. Settu, A. Basu, and S. K. Koul, "Novel mechanical reconfigurable PCB antenna for 2.4 GHz wireless consumer product: Minimizing time to market," in *Proc. 3rd Asia–Pacific Conf. Antennas Propag. (APCAP)*, Harbin, China, Jul. 2014, pp. 18–21.

[22] L. Pazin, N. Telzhensky, and Y. Leviatan, "Multiband flat-plate inverted-F antenna for Wi-Fi/WiMAX operation," *IEEE Antennas Wireless Propag. Lett.*, vol. 7, pp. 197–200, 2008.

[23] Y.-L. Kuo, T.-W. Chiou, and K.-L. Wong, "A novel dual-band printed inverted-F antenna," *Microw. Opt. Technol. Lett.*, vol. 31, no. 5, pp. 353–355, Dec. 2001.

[24] X. L. Sun, L. Liu, S. W. Cheung, and T. I. Yuk, "Dual-band antenna with compact radiator for 2.4/5.2/5.8 GHz WLAN applications," *IEEE Trans. Antennas Propag.*, vol. 60, no. 12, pp. 5924–5931, Dec. 2012.

[25] M. Gallo, O. Losito, V. Dimiccoli, D. Barletta, and M. Bozzetti, "Design of an inverted F antenna by using a transmission line model," in *Proc. 5th Eur. Conf. Antennas Propag. (EUCAP)*, Rome, Italy, Apr. 2011, pp. 635–638.

[26] B. Gowrish, R. Kumar, and A. Basu, "Radiation enhancement in PCB plane using novel multi-stub inverted f antenna," in *Proc. IEEE Annu. India Conf. (INDICON)*, Bengaluru, India, Dec. 2016, pp. 1–4.

[27] J. Tie-Hua, S. Dong-Lin, D. Ke-Jia, W. Guo-Yu, and Z. Yan, "Design of the low-profile inverted-F antenna with multiparasitic elements," in *Proc. 7th Int. Symp. Antennas Propag. EM Theory*, Guilin, China, Oct. 2006, pp. 1–4.

[28] B. Desplanches, A. Sharaiha, and C. Terret, "Parametrical study of printed quadrifilar helical antennas with central dielectric rods," *Microw. Opt. Technol. Lett.*, vol. 20, no. 4, pp. 249–255, Feb. 1999.

[29] D. K. C. Chew and S. R. Saunders, "Meander line technique for size reduction of quadrifilar helix antenna," *IEEE Antennas Wireless Propag. Lett.*, vol. 1, pp. 109–111, 2002.

[30] Y. Letestu, A. Sharaiha, and P. Besnier, "A size reduced configurations of printed quadrifilar helix antenna," in *Proc. IEEE Int. Workshop Antenna Technol., Small Antennas Novel Metamater. (IWAT)*, Singapore, Mar. 2005, pp. 326–328.

[31] M. Amin and R. Cahill, "Effect of helix turn angle on the performance of a half wavelength quadrifilar antenna," *IEEE Microw. Wireless Compon. Lett.*, vol. 16, no. 6, pp. 384–386, Jun. 2006.

[32] G. Byun, H. Choo, and S. Kim, "Design of a dual-band quadrifilar helix antenna using stepped-width arms," *IEEE Trans. Antennas Propag.*, vol. 63, no. 4, pp. 1858–1862, Apr. 2015.

[33] X.-F. Wang, X.-J. Li, H. Wang, and S.-G. Zhou, "Design of a compact and wideband quadrifilar helix antenna," in *Proc. IEEE Asia–Pacific Conf. Antennas Propag. (APCAP)*, Auckland, New Zealand, Aug. 2018, pp. 68–69.

[34] W. Qin, L.-H. Shi, W.-J. Sun, W.-W. Yang, L. Ge, and J.-X. Chen, "A wideband LTCC quad-phase power dividing network and its application to ceramic-based quadrifilar helix antennas," *IEEE Access*, vol. 7, pp. 141094–141103, 2019.

[35] Y. Han, H. Wang, Z. Wang, Y. Yao, Y. Feng, K. Hu, Y. Gao, Z. Fan, and S. Yuan, "Dual-band spiral printed quadrifilar helical antenna miniaturized by surface and inner dielectric loading," *IEEE Access*, vol. 7, pp. 30244–30251, 2019.

[36] Ansys, Canonsburg, PA, USA. (2018). *HFSS V19.2*. [Online]. Available: https://www.ansys.com

[37] A. Motevasselian, A. Ellgardt, and B. L. G. Jonsson, "A helix excited circularly polarized hollow cylindrical dielectric resonator antenna," *IEEE Antennas Wireless Propag. Lett.*, vol. 12, pp. 535–538, 2013.

YUNAN HAN (Member, IEEE) received the Ph.D. degree in electromagnetic and microwave technology from the Beijing University of Posts and Telecommunications, Beijing, China, in 2007. After working at the China Academy of Launch Vehicle Technology for three years, he joined the College of Information Science and Technology, Beijing University of Chemical Technology, where he is currently an Associate Professor. From 2013 to 2014, he was a Visiting Scholar with the Electromagnetic Compatibility Laboratory, Missouri University of Science and Technology. He is certificated iNARTE MIL-STD EMC Specialist, in 2014. His main research interests are EMC, ESD, EMP, and microwave devices design.

KUNKUN HU was born in Anqing, Anhui, China. He received the bachelor's degree in communication engineering from the Beijing University of Chemical Technology, in 2018, where he is currently pursuing the master's degree in control engineering. His research interests focus on the microwave engineering and antenna design.

RUICHUN ZHAO was born in Baotou, China. She is currently studying with the College of Materials Science and Engineering, Beijing University of Chemical Technology. She is majoring in materials science and engineering.

YUAN GAO was born in Beijing, China. He received the bachelor's degree in communication engineering from the Beijing University of Chemical Technology, in 2018. He is currently pursuing the degree in electronics and communication engineering with North China Electric Power University. He specialized in intelligent information processing and information security.

LIN DAI was born in Panjin, Liaoning, China. She received the master's degree in communication engineering from Northeast Petroleum University, in 2014. She is currently working in wireless sense network and information security with the Liaohe Oilfield of China National Petroleum Corporation.

YUFENG FU was born in Jinhua, Zhejiang. He is currently studying with the Beijing University of Chemical Technology. He is also majors in communication engineering with the College of Information Science and Technology.

BOWEN ZHOU was born in Taiyuan, Shanxi. He is currently studying with the Beijing University of Chemical Technology. He majors in communication engineering with the College of Information Science and Technology.

SIYU YUAN was born in Beijing, China. He is currently pursuing the Ph.D. degree in electric engineering with the Beijing University of Posts and Telecommunications. His research directions are wireless communications, electric engineering, and antenna design.